



# Determination of the Thresholds in the Split-Step Wavelet Method to Assess Accuracy for Long-Range Propagation

Thomas Bonnafont, Rémi Douvenot, Alexandre Chabory

## ► To cite this version:

Thomas Bonnafont, Rémi Douvenot, Alexandre Chabory. Determination of the Thresholds in the Split-Step Wavelet Method to Assess Accuracy for Long-Range Propagation. *URSI Radio Science Letters*, 2021, 3, 10.46620/21-0009 . hal-03693958

**HAL Id: hal-03693958**

**<https://hal.science/hal-03693958>**

Submitted on 3 Jan 2023

**HAL** is a multi-disciplinary open access archive for the deposit and dissemination of scientific research documents, whether they are published or not. The documents may come from teaching and research institutions in France or abroad, or from public or private research centers.

L'archive ouverte pluridisciplinaire **HAL**, est destinée au dépôt et à la diffusion de documents scientifiques de niveau recherche, publiés ou non, émanant des établissements d'enseignement et de recherche français ou étrangers, des laboratoires publics ou privés.

# Determination of the thresholds in split-step wavelet to assess accuracy for 2D long-range propagation

Thomas Bonnafont, Rémi Douvenot, and Alexandre Chabory

**Abstract** – Split-step wavelet is a method for computing the tropospheric long-range propagation of electromagnetic waves. It follows the same steps as split-step Fourier, but the propagation is performed in the wavelet domain instead of the Fourier domain. The efficiency of the method is based on the fast wavelet transform of low complexity and on the sparse representation using compression. Nevertheless, the compression introduces an error that accumulates while iterating. In this paper, we propose a closed-form formula for the error that allows to compute *a priori* the compression thresholds for a given scenario and accuracy. Numerical experiments show the relevance of the proposed approach.

## 1. Introduction

The tropospheric long-range propagation is a topic of major interest for a large number of applications in communication, surveillance, and navigation. The parabolic wave equation (PWE) model [1] is widely used in this context. In the literature, the PWE is iteratively solved with split-step Fourier (SSF) by going back and forth in the spectral and spatial domain [2, 3]. This method allows to make large steps in the propagation direction [1].

To accelerate the computation, wavelet-based methods have been proposed in optics [12] and electromagnetics [5-7]. Recently, an efficient split-step wavelet method (SSW) [6, 7, 15] has been introduced to solve the PWE in electromagnetics in both 2D and 3D. This method computes the field by marching on in distances as SSF, but the propagation is performed in the wavelet domain instead of the spectral domain. Each iteration follows two steps. First, the field is decomposed in the wavelet domain and compressed, introducing the signal compression error (threshold  $V_s$ ). Second, the coefficients are propagated using a compressed wavelet-to-wavelet propagator, introducing the propagator compression error (threshold  $V_p$ ). These errors accumulate throughout the propagation and need to be quantified. Indeed, Zhou *et al.* [6] have shown that SSW is faster than SSF if a good compression is performed.

The main contribution of this letter is that we derive a theoretical formula of the accumulated compression error after  $N_x$  iterations. This allows to set both thresholds *a priori* for a given accuracy and scenario. We also show

that the heuristic formula proposed in earlier works [6, 10] is too optimistic.

For conciseness, the method and the proof are developed in 2D. Nevertheless, the results remain valid in 3D using similar calculations. After a general presentation of SSW (Section 2), the error formula is derived (Section 3) and tested via numerical experiments (Section 4) in 2D.

## 2. Overview of split-step wavelet

### 2.1. Configuration and discretization

In this article, an  $\exp(j\omega t)$  time dependence is assumed, where  $\omega$  is the angular frequency. The domain is 2D of size  $[0, x_{\max}]$  in  $x$  and  $[0, z_{\max}]$  in  $z$ . The field is known at  $x = 0$  and the source is placed at  $x \leq 0$ . On the  $z$ -axis a sampling is made with  $z_{p_z} = p_z \Delta z$  and  $p_z \in \{0, \dots, N_z - 1\}$ . On the  $x$ -axis a sampling is made with  $x_{p_x} = p_x \Delta x$  and  $p_x \in \{0, \dots, N_x - 1\}$ .

### 2.2. Brief reminder of the discrete wavelet transform

The wavelet family is computed by dilating and translating a mother wavelet of zero mean on  $L$  levels [4]. Dilations allow covering the lower parts of the spectrum. To obtain an orthonormal basis, a scaling function of non-zero mean is added. This function covers the lowest part of the spectrum. Using this basis, a multi-level decomposition is obtained. We recall one important property of the wavelets used in the following demonstrations. The number of vanishing moments  $n_v$  of a wavelet  $\psi$  is defined as

$$\forall k \in [0, n_v], \int z^k \psi(z) dz = 0. \quad (1)$$

This property describes how well a wavelet decomposition can approach a smooth function with few coefficients.

### 2.3. An overview of SSW

SSW computes the field iteratively by going back and forth from the wavelet to the spatial domains. As for the SSF, the refraction and relief are taken into account in the spatial domain, thus we only describe the free-space propagation part. The initial field  $u_0$  is supposed known.

Denoting  $u_{p_x}$  the field and  $U_{p_x}$  its wavelet decomposition at distance  $p_x \Delta x$ , a step of SSW is computed as follows. First the wavelet coefficients  $U_{p_x}$  are computed by applying a FWT on  $u_{p_x}$  (denoted  $\mathbf{W}$ ). Then, the coefficients are compressed (operator  $C_{V_s}$ ) with a hard threshold  $V_s$  (*i.e.*, all coefficients below  $V_s$  are set to 0). A sparse vector of size  $N_z$  is obtained. This first compression repeated on  $N_x$  horizontal steps induces an error term denoted by  $\delta_{N_x}^s$ .

Then, the coefficients are propagated using a pre-computed matrix  $\mathbf{P}$

$$U_{p_x+1} = \mathbf{P}C_{V_s}U_{p_x}. \quad (2)$$

This sparse matrix contains all the wavelet-to-wavelet propagations and is of size  $(N_z, N_z)$  [6]. A compression with hard threshold  $V_p$  is performed. Iterated  $N_x$  times, this second term of error in the method is denoted by  $\delta_{N_x}^m$ . The free-space propagated field is obtained by coming back in the space domain using an inverse FWT. The total compression error is denoted by  $\delta_{N_x} = \delta_{N_x}^s + \delta_{N_x}^m$ .

In [6] the experimental upper bound was supposed to be of order  $N_x^{0.5}V_s$  and  $N_xV_p$  for the signal and propagator compressions, respectively. We derive here new and more accurate expressions.

### 3. Derivation of the compression error formula

In the following section, we introduce the normalised thresholds  $v_s$  and  $v_p$  such that  $V_s = v_s\|U_0\|_\infty$  and  $V_p = v_p\|\mathbf{P}\|_{\max}$  [4, 8]. We also remind that the operator norm of  $\mathbf{P}$  corresponds to

$$\|\mathbf{P}\|_{\text{op}} = \sup_{U \neq 0} \|\mathbf{P}U\|_2 / \|U\|_2. \quad (3)$$

From power conservation, the operator norm of the free-space propagator  $\mathbf{P}$  is equal to 1 ( $\|\mathbf{P}\|_{\text{op}} = 1$ ). If there are no evanescent waves and the propagation does not reach any boundaries, then we have  $\|\mathbf{P}u\|_2 = \|u\|_2$ . In other cases (apodization, environment losses, evanescent waves, ...), then we have  $\|\mathbf{P}u\|_2 \leq \|u\|_2$ .

#### 3.1. Signal compression error

The objective of this section is to study how the signal compression error accumulates with  $N_x$ . We first assume that  $V_s \neq 0$  and  $V_p = 0$ . The propagator has no compression. The error due to the threshold  $V_s$  on signal (operator  $C_{V_s}$ ) after  $N_x$  iterations is defined by

$$\delta_{N_x}^s = \|\tilde{U}_{N_x} - U_{N_x}\|_2 / \|U_0\|_2, \quad (4)$$

with  $\tilde{U}_{N_x} = (\mathbf{P}C_{V_s})^{N_x}U_0$  and  $U_{N_x} = \mathbf{P}^{N_x}U_0$  the compressed and uncompressed propagated coefficients, respectively.

For one iteration, the error is given by

$$\delta_1^s = \|\mathbf{P}C_{V_s}U_0 - \mathbf{P}U_0\|_2 / \|U_0\|_2. \quad (5)$$

We introduce  $\varepsilon^0$  the compression term due to  $C_{V_s}$  defined by

$$C_{V_s}U_0 = U_0 + \varepsilon^0. \quad (6)$$

Using (3) and introducing (6) in (5) we obtain  $\delta_1^s \leq \|\varepsilon^0\|_2 / \|U_0\|_2$ . For the smooth signals we are manipulating the wavelet coefficients decrease exponentially to 0 [4, 8]. Therefore, we rewrite the norm of the error as follows

$$\|\varepsilon\|_2^2 = v_s^2 \|U_0\|_\infty^2 \sum_{m=0}^{N_z-M-1} |\hat{\varepsilon}_m^0|^2, \quad (7)$$

with the coefficients  $|\hat{\varepsilon}_m^0| \leq 1$  corresponding to the normalised amplitudes of the wavelet coefficients of the error indexed in decreasing order, and  $M \ll N_z$  the number of significant coefficients. Following [4, 8, 9], error components are bounded by

$$|\hat{\varepsilon}_m^0| \leq C_\varepsilon (m+1)^{-n_v}, \quad (8)$$

with  $m \in [0, N_z - M - 1]$ ,  $n_v$  the number of vanishing moments and  $C_\varepsilon$  a constant depending only on the smoothness of the field and of the wavelets. Putting (8) in (7), an upper bound for  $\|\varepsilon_0\|_2$  is obtained

$$\|\varepsilon^0\|_2 \leq v_s \|U_0\|_\infty C_\varepsilon \sqrt{\sum_{m=0}^{N_z-M-1} (m+1)^{-2n_v}}. \quad (9)$$

For  $n_v \geq 2$  the sum converges close to 1 (*e.g.* for  $n_v = 2$  the sum is about 1.082). Also,  $C_\varepsilon$  is inferior or close to 1 as illustrated with numerous numerical tests in Section 4 and in [14].

Thus, the bound on the error due to signal compression after one iteration is given by

$$\|\varepsilon^0\|_2 \lesssim v_s \|U_0\|_2 \quad \text{and} \quad \delta_1^s \lesssim v_s, \quad (10)$$

where  $\lesssim$  means inferior or close to as widely used in the wavelet community [4, 8]. In practice, this result shows a very good accuracy with numerous numerical tests performed in [6, 11].

For 2 iterations, we compare the propagations with and without compression

$$\delta_2^s = \|(\mathbf{P}C_{V_s})(\mathbf{P}C_{V_s})U_0 - \mathbf{P}\mathbf{P}U_0\|_2 / \|U_0\|_2. \quad (11)$$

We define the second compression error  $\varepsilon^1$  such as  $C_{V_s}(\mathbf{P}U_0 + \mathbf{P}\varepsilon^0) = \mathbf{P}U_0 + \mathbf{P}\varepsilon^0 + \varepsilon^1$ . The expression of the error is calculated as

$$\begin{aligned} \delta_2^s &= \|\mathbf{P}\mathbf{P}U_0 + \mathbf{P}\mathbf{P}\varepsilon^0 + \mathbf{P}\varepsilon^1 - \mathbf{P}\mathbf{P}U_0\|_2 / \|U_0\|_2, \\ &\leq (\|\varepsilon^0\|_2 + \|\varepsilon^1\|_2) / \|U_0\|_2. \end{aligned} \quad (12)$$

Supposing (10) is true for the 2nd iteration, we obtain

$$\|\epsilon^1\|_2/\|U_0\|_2 \lesssim v_s(\|U_0\|_2 + \|\epsilon^0\|_2)/\|U_0\|_2. \quad (13)$$

Since, with appropriate threshold,  $\|\epsilon^0\|_2$  is negligible to  $\|U_0\|_2$ , we have  $\delta_2^s \lesssim 2v_s$ . By induction, the signal compression error after  $N_x$  horizontal iterations fulfills

$$\delta_{N_x}^s \lesssim N_x v_s. \quad (14)$$

The appropriate threshold  $V_s = v_s \|U_0\|_\infty$  can now be computed with (14). The same study is now performed on the error due to the compression of the propagator  $\mathbf{P}$  in (2).

### 3.2. Propagator compression error

We now assume that  $V_s = 0$  and  $V_p \neq 0$ . The error  $\delta_{N_x}^p$  due to the compression of the propagator after  $N_x$  iterations is studied. It is defined by

$$\delta_{N_x}^p = \|\tilde{U}_{N_x} - U_{N_x}\|_2/\|U_0\|_2, \quad (15)$$

where  $\tilde{U}_{N_x}$  corresponds to the coefficients propagated  $N_x$  times with the compressed operator denoted as  $\mathbf{P} + \Delta\mathbf{P}$ .

From [8, pp 29–32], we have the norm operator of  $\Delta\mathbf{P}$  bounded by

$$\|\Delta\mathbf{P}\|_{\text{op}} = \sup_{U \neq 0} \|\Delta\mathbf{P}U\|_2/\|U\|_2 \leq v_p. \quad (16)$$

For one iteration the expression of the error is given by

$$\delta_1^p = \|\tilde{U}_1 - U_1\|_2/\|U_0\|_2 = \|\Delta\mathbf{P}U_0\|_2/\|U_0\|_2. \quad (17)$$

Following (16), we have  $\delta_1^p \leq v_p$ . This result is in line with the one obtained for optics [12].

Using the same notations and methodology as for 1 iteration and since  $\|\mathbf{P}\|_{\text{op}} = 1$ , we obtain for 2 iterations using (16)

$$\begin{aligned} \delta_2^p &= \|\tilde{U}_2 - U_2\|_2/\|U_0\|_2, \\ &\leq \frac{\|\Delta\mathbf{P}\mathbf{P}U_0\|_2 + \|\mathbf{P}\Delta\mathbf{P}U_0\|_2 + \|\Delta\mathbf{P}^2U_0\|_2}{\|U_0\|_2}, \\ &\leq 2v_p + v_p^2. \end{aligned} \quad (18)$$

Neglecting the term  $v_p^2$  ( $v_p \ll 1$ ),  $\delta_2^p$  is shown to be smaller than or close to  $2v_p$ . By induction, we finally obtain

$$\delta_{N_x}^p \lesssim v_p N_x. \quad (19)$$

Formula (19) allows to choose the adequate threshold  $V_p$  for a given error and scenario.

Assuming that both errors are independent, we finally derive a closed-form expression for the accumulated compression error  $\delta_{N_x} \lesssim (v_s + v_p)N_x$ . In practice,

for a given maximum expected error  $\delta_{N_x}^{\text{max}}$  and number of iterations  $N_x$ , the normalised thresholds are computed as

$$v_s = \delta_{N_x}^{\text{max}}/(2N_x) \text{ and } v_p = \delta_{N_x}^{\text{max}}/(2N_x). \quad (20)$$

Thus, we derive the unnormalised thresholds

$$V_s = \frac{\delta_{N_x}^{\text{max}}}{2N_x} \|U_0\|_\infty \text{ and } V_p = \frac{\delta_{N_x}^{\text{max}}}{2N_x} \|\mathbf{P}\|_{\text{max}}. \quad (21)$$

## 4. Numerical tests

In this part, numerical experiments are performed to show that the thresholds  $v_s$  and  $v_p$  can be managed to assess a given final accuracy for a certain number of iterations  $N_x$ , using expressions (20). First, a short-range simulation in free-space is performed to assess the accuracy of the formulas. Second, we perform a long-range simulation with relief and refraction.

### 4.1. Free-space scenario

We perform the tests in 2D. The source is a uniform aperture at  $f_0 = 300$  MHz of size 10 m and is placed at  $z_s = 1024$  m in a domain of vertical size  $z_{\text{max}} = 2048$  m. The domain is of horizontal size  $x_{\text{max}} = 2000$  m. The steps are  $\Delta x = 20$  m and  $\Delta z = 0.5$  m. Thus, we have  $N_x = 100$ . For the wavelet parameters, the symlet with  $n_v = 6$  and a maximum level of  $L = 3$  are chosen.

The RMS error between compressed and uncompressed propagations is computed for different values of  $N_x$  and compared to the closed-form formulas. Thresholds are set to  $v_s = v_p = 1.6 \times 10^{-4}$  using (20) so as to obtain an error of  $-30$  dB at the final range.

First, we compute and plot in Figure 1 the constant  $C_\epsilon \simeq \|\epsilon\|_2/V_s$  at each step  $N_x$ . This shows that the constant is inferior to or close to 1. Indeed, in this case, the field is smooth. The approximation proposed in Section 3.1 is relevant.

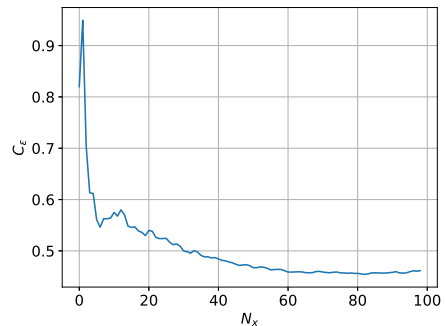


Figure 1: Evolution of  $C_\epsilon$  with  $N_x$ .

The RMS error is computed and given in Figure 2. As expected, Figure 2 shows that the closed-form formula

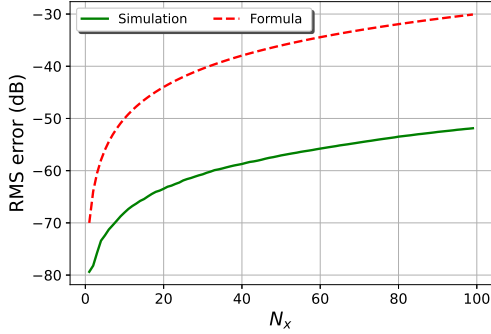


Figure 2: Evolution of the RMS error.

for the compression error is never reached. The computed thresholds allow to bound the error below the desired maximum. We also compute a linear regression to find the optimal  $\alpha$  such that  $\delta_{N_x}^s \sim v_s N_x^\alpha$  and  $\delta_{N_x}^p \sim v_p N_x^\alpha$ . For the signal compression, we obtain  $\alpha = 0.96$  slightly lower than the value proposed here, *i.e.*, 1, but greater than the heuristic value proposed in [6], *i.e.*, 0.5. This shows that the heuristic formula proposed in [6] was too optimistic. For the propagator,  $\alpha = 0.97$  is obtained, close to the value proposed here and in [6].

Numerical tests show the relevancy of the proposed formulas (20). Therefore, it can be used to tune the thresholds needed in SSW to obtain a given accuracy. In the next section, a numerical test in realistic conditions is performed.

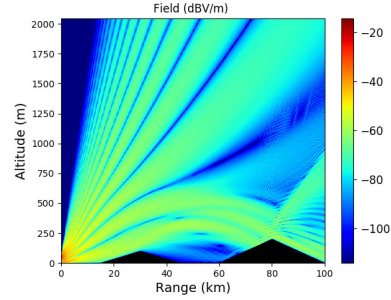
#### 4.2. Realistic scenario

The propagation of a complex source point (CSP) in a domain with a trilinear atmosphere and two triangular reliefs is computed. The CSP parameters are: a frequency  $f = 300$  MHz, with coordinates  $x_{w0} = -50$  m and  $z_s = 50$  m, with a waist size of  $W_0 = 5$  m. We consider an atmosphere described by a trilinear duct [13] of base height  $z_b = 241$  m, thickness  $z_t = 391$  m and gradient  $c_2 = -0.5$  M-units/m in the duct and  $c_0 = 0.118$  M-units/m elsewhere. On the ground, we choose  $M_0 = 330$  M-units. The relief is chosen as 2 small triangles of heights 100 m and 200 m. The impedance ground is of parameters  $\epsilon_r = 20.0$  and  $\sigma = 0.02$  S/m.

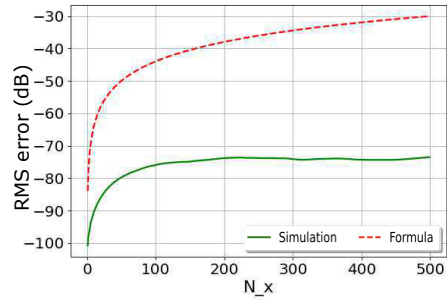
The domain is of size  $x_{\max} = 100$  km in horizontal and  $z_{\max} = 2048$  m in vertical. An apodization window is added on top of the domain. The grid size is 200 m in horizontal and 0.5 m in vertical. We aim at obtaining an error of  $-30$  dB at the final iteration. From (20) we apply the thresholds  $v_s = v_p = 3.16 \times 10^{-5}$ .

In Figure 3, the field in dBV/m is plotted in (a) and the RMS error evolution is plotted in (b). We can see that

the bound is not reached and that the final error is significantly smaller than the desired error. This is mostly due to the apodization layer in which energy is leaving the computational domain, reducing the total error. Therefore, our formula is conservative in a realistic domain, as expected.



(a) Field obtained with SSW (dBV/m).



(b) RMS error (dB).

Figure 3: Results for the realistic test case.

## 5. Conclusion

In this letter, we have derived a closed-form expression for the accumulated compression error in split-step wavelet (SSW). This formula allows to tune the thresholds  $V_s$  and  $V_p$  for a given accuracy.

First, we have given an overview of SSW to show where thresholds are applied. The compressions on the signal  $V_s$  on the propagator  $V_p$  introduce errors. We derived how each error accumulates while iterating to obtain a closed-form expression for the compression error. This latter allows to set *a priori*  $V_s$  and  $V_p$  for a given accuracy and scenario. Finally, numerical tests in 2D have been performed. Our proposed bounds are never reached, as expected, which shows their relevancy.

To conclude, the expression obtained in this article for the accumulated compression error is used in SSW [15] to tune  $V_s$  and  $V_p$  for a given accuracy.

## 6. References

1. M. Levy, *Parabolic Equation Methods for Electromagnetic Wave Propagation*, IET, 2000.
2. D. Dockery, and J.R. Kuttler, "An improved impedance-boundary algorithm for Fourier split-step solutions of the parabolic wave equation," *IEEE Transactions on Antennas and Propagation*, **44**, 12, 1996, pp. 1592-1599.
3. J.R. Kuttler, and R. Janaswamy, "Improved Fourier transform methods for solving the parabolic wave equation," *Radio Science*, **37**, 2, 2002, pp. 1-11.
4. S. Mallat, *A Wavelet Tour of Signal Processing*, Academic Press, 1999.
5. A. Iqbal, and V. Jeoti, "An improved split-step wavelet transform method for anomalous radio wave propagation modeling," *Radioengineering*, **23**, 4, 2014, pp. 987.
6. H. Zhou, R. Douvenot, and A. Chabory, "Modeling the long-range wave propagation by a split-step wavelet method," *Journal of Computational Physics*, **402**, 2020, pp. 109042.
7. T. Bonnafont, R. Douvenot, and A. Chabory, "A local split-step wavelet method for the long range propagation simulation in 2D," *Radio Science*, **56**, 2021, pp. e2020RS007114.
8. A. Cohen, *Numerical Analysis of Wavelet Methods*, Elsevier, 2003.
9. R. A. DeVore, B. Jawerth, and V. Popov, "Compression of wavelet decompositions," *American Journal of Mathematics*, **114**, 4, 1992, pp. 737-785.
10. H. Zhou, "Modeling the atmospheric propagation of electromagnetic waves in 2-D and 3-D using Fourier and wavelet transforms," PhdThesis, Université Paul Sabatier - Toulouse III, 2018.
11. T.K. Sarkar, M. Salazar-Palma, and M.C. Wicks, *Wavelet Applications in Engineering Electromagnetics*, Artech House, 2002
12. T. Kremp, and W. Freude, "Fast split-step wavelet collocation method for WDM system parameter optimization," *Journal of Lightwave Technology*, **23**, 3, 2005, pp. 1481-1502.
13. E.E. Gossard and R.G. Strauch, "Radar observation of clear air and clouds," *Developments in Atmospheric Science*, **14**, 1983.
14. T. Bonnafont, "Modeling the atmospheric long-range electromagnetic waves propagation in 3D using the wavelet transform," PhdThesis, Université Paul Sabatier - Toulouse III, 2020.
15. T. Bonnafont, R. Douvenot, and A. Chabory, "Split-step wavelet with local operators for the 3D long-range propagation," *2021 15th European Conference on Antennas and Propagation (EUCAP)*, 2021, pp. 1-5

Thomas Bonnafont was with ENAC, Université de Toulouse, France (now with ENSTA Bretagne), 7 avenue Edouard Belin, Toulouse, France ; e-mail: thomas.bonnafont@ensta-bretagne.fr.

Rémi Douvenot is with ENAC, Université de Toulouse, France, 7 avenue Edouard Belin, Toulouse, France; e-mail: remi.douvenot@enac.fr.

Alexandre Chabory is with ENAC, Université de Toulouse, 7 avenue Edouard Belin, Toulouse, France ; e-mail: alexandre.chabory@enac.fr.